Universal scaling laws in turbulent Rayleigh-Bénard convection with and without roughness

Lyse Brichet, Nathan Carbonneau, Elian Bernard, Romane Braun, Lucas Méthivier, Yann Fraigneau, Didier Lucor, Francesca Chillà, Anne Sergent, Julien Salort

Universal scaling laws in turbulent Rayleigh-Bénard convection with and without roughness

Lyse Brichet[1], Nathan Carbonneau[2], Elian Bernard[1], Romane Braun[1], Lucas Méthivier[1], Yann Fraigneau[2], Didier Lucor[2], Francesca Chillà[1], Anne Sergent[2,3], and Julien Salort[1*]
[1] *ENSL, CNRS, Laboratoire de physique, F-69342 Lyon, France.*
[2] *Université Paris-Saclay, CNRS, LISN, F-91400 Orsay, France. and*
[3] *Faculté des Sciences et Ingénierie, UFR d'Ingénierie, Sorbonne Université, F-75005 Paris, France.*
(Dated: July 10, 2024)

Experimental heat-transfer measurements published in the literature seem to be contradictory, some showing a transition at $Ra \approx 10^{11}$, some showing a delayed transition at higher Ra, or no transition at all. New experimental and numerical heat-flux and velocity measurements, both reaching Ra up to 10^{12}, are reported on a wide range of operating conditions. In the new measurements in the rough cell which reaches Rayleigh numbers, Ra, up to 2.5×10^{12}, the Nusselt number show a clear $Ra^{1/2}$ scaling, hinting a fully turbulent regime. In contrast to the Nu *vs* Ra relationship, we evidence that the dimensionless heat-flux, expressed as $RaNu$, recovers a universal scaling with Reynolds number, collapses all data and highlights a universal critical Reynolds number.

Turbulent Rayleigh-Bénard Convection (RBC) is a model system where a layer of fluid is heated from below and cooled from above. It is controlled by three dimensionless parameters: the Rayleigh number Ra,

$$Ra = \frac{g\alpha\Delta T H^3}{\nu\kappa}, \tag{1}$$

the Prandtl number Pr,

$$Pr = \frac{\nu}{\kappa}, \tag{2}$$

and the aspect ratio $\Gamma = L/H$, where g is the acceleration of gravity, α the thermal expansion coefficient, ΔT the temperature difference across the fluid layer, ν the kinematic viscosity, κ the thermal diffusivity, H the height of the cell, and L the width of the cell. A long standing endeavor consists in finding universal scaling laws for the heat transfer, expressed as the dimensionless parameter Nusselt number Nu [1, 2],

$$Nu = \frac{\dot{q}H}{\lambda\Delta T}, \tag{3}$$

where $\dot{q}$ is the heat-flux, and λ the thermal conductivity. This would allow extrapolating results from laboratory experiments to natural systems where highly turbulent natural convection plays a role. These include in particular convection in the ocean at the pole or in subglacial lakes [3], resulting in Rayleigh numbers beyond 10^{14}, and in the "ultimate regime" of convection where $Nu \sim Ra^{1/2}$ (with logarithmic corrections) [4]. However, experimental heat-transfer measurements published in the literature for $Ra > 10^{11}$ seem to be contradictory, some showing a transition at $Ra \approx 10^{11}$ [5, 6], some showing a delayed transition at higher Ra [7], or no transition at all [8, 9]. These experiments are within Oberbeck-Boussinesq conditions [10] and share similar geometries, but differ in Prandtl numbers and details in the setup. It now seems clear that the transition to the ultimate regime may be a subcritical process, and may depend on aspect ratio and Prandtl numbers [11–13].

In this letter, we evidence a way to recover universality. We report new velocity data obtained from shadowgraph imaging in parallelepiped Rayleigh-Bénard cells with or without roughness and using either deionized water or Fluorocarbon FC-770 as the working fluid. The cell dimensions are 41.5 cm × 41.5 cm × 10.5 cm for the aspect ratio 1 cell, and 20 cm × 41.5 cm × 10.5 cm for the aspect ratio 2 cell. The details of the cell are described in [14]. The Rayleigh number spans a wide range between 10^9 and 2.5×10^{12}, the Prandtl number between 4.3 and 7.0 in water, and 11 and 14 in FC-770, and the aspect ratio 1 or 2.

In addition, direct numerical simulations (DNS) were carried out in a similar geometric configuration filled with water. Two cavities with depth to width aspect ratios Γ_{xy} of one-half and one-quarter, and height to width aspect ratio $\Gamma_{xz} = 1$ have been modeled. Rayleigh numbers range from 5×10^8 to 10^{12}. Details of the numerical code can be found in [15].

In these conditions, the flow can be quite different, the scaling exponent of Nu *versus* Ra also quite different, and in apparent disagreement with data from Grenoble, Oregon, Brno and Göttingen cited above. And yet, all the data can be collapsed using the appropriate scaling of Reynolds and Prandtl numbers.

The experimental cells can be set up with roughness on the bottom plate, consisting in square roughness elements of height $h_0 = 2$ mm, machined in the plate, as described in [16]. In the DNS, three surface states for the bottom wall have been modeled: smooth or rough wall with two roughness heights ($h_0/H = 0.04$ or 0.003). In the rough cases, the cell (later referred to as "RS"), is asymmetrical, with a rough bottom plate, and a smooth top plate. As shown in our previous works [17, 18], this allows to define Rayleigh and Nusselt numbers of the rough and smooth half cells, provided the bulk temperature T_{bulk}

is also known. The temperature drop across the boundary layer of the smooth plate, $\Delta T_s = T_{\text{bulk}} - T_{\text{top}}$, and the temperature drop across the boundary layer of the rough plate, $\Delta T_r = T_{\text{bottom}} - T_{\text{bulk}}$ allow to estimate the total temperature difference across a corresponding virtual symmetric cell with identical smooth plates as $2\Delta T_s$, or with identical rough plates as $2\Delta T_r$, from which Ra_s, Nu_s, Ra_r, Nu_s are derived.

The experimental smooth cell (later referred to as "SS") has entirely smooth boundaries, as described in [14]. We have now operated the experimental rough configuration (RS) with Fluorocarbon FC-770 thus significantly extending the previous heat-transfer results in water [19], see Figure 1. In the Fluorocarbon cell, the thermal boundary layer, estimated as $\delta_{th} = H/(2Nu)$, ranges between 250 µm and 500 µm, much smaller than the roughness height h_0. The kinetic boundary layer, estimated as $\delta_v \approx \delta_{th} Pr^{1/3}$ ranges between 600 µm and 1100 µm, smaller than the roughness height h_0. Therefore, the rough cell lies in Regime III as defined by Xie & Xia [20]. By the same definition, DNS configurations can be either in Regime II or Regime III. At $Ra = 10^{10}$, the simulation with the smaller roughness size ($h_0/H = 0.003$) is in Regime II, while the simulation with the larger roughness size ($h_0/H = 0.04$) is in Regime III.

Even when the rough half-cell has a $Ra^{1/2}$ scaling, the smooth half-cell is in good agreement, over more than 3 decades of Rayleigh numbers, with heat-transfer measurements in SS cell, as well as with the Grossmann-Lohse model [2]. This shows that the top and bottom plates remain independent, even very far from the roughness-triggered enhancement threshold, and holds even when the Nusselt number of the bottom half is nearly twice as large as that of the top half. This is a major result that shows how the boundary layers adapt themselves to maintain the heat-flux constant.

We computed the velocity fields using *Correlation Image Velocimetry* on shadowgraph recordings for all of them, yielding consistent estimates for both the mean and fluctuation velocities, as well as consistent Reynolds number estimates in all configurations. The method consists in deriving velocity estimates from the shadowgraph pattern using the same algorithm we use for *Particle Image Velocimetry* (PIV) images, i.e. the image is divided into smaller boxes that are correlated at t and $t + \Delta t$, the displacement that produce the maximum correlation is used as an estimate for the local velocity. This method, based on the shadowgraph pattern, has previously been validated against standard PIV in experimental conditions where both were possible [14]. One should be aware that the shadowgraph patterns result from the deviation of light across the cell depth. Therefore, the obtained velocity is integrated over the depth, in contrast to PIV which is computed on a plane.

While we find that the mean flow has the same structure at $Ra = 10^{10}$ and $Ra = 10^{12}$, the velocity fluctuations differ, see Figure 2. At higher Rayleigh numbers, and in this range of Prandtl where we do not see evidence for a transition to the ultimate regime, we find that the velocity fluctuations are globally much larger, and also more focused near the impinging jets than in the lower Rayleigh number case.

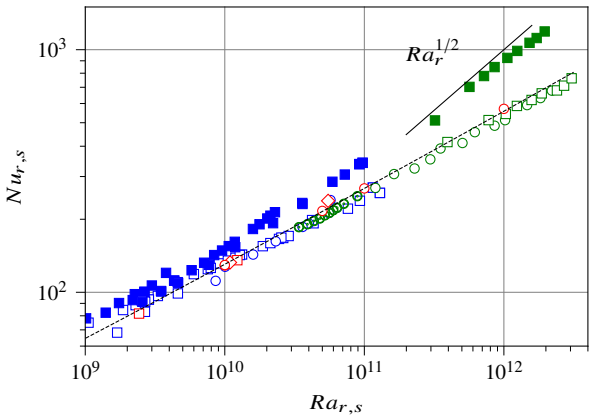

FIG. 1. Heat-transfer measurements. Blue: deionized water. Green: Fluorocarbon FC-770. Red: DNS. Full squares: rough half-cell of RS cell. Open squares: smooth half-cell of RS cell. Circles: SS cell. Circles with center dot: SS cell with $\Gamma = 2$. RS cell in water from [19]. SS cells in FC-770 from [14]. SS cell in water, RS cell in FC-770 and DNS: new data. Solid black line: $Ra^{1/2}$. Dashed black line: Grossmann-Lohse model [2]

When roughness is added to the bottom plate, mean velocity is increased between 5 % and 20 % in the range of parameters explored in this work, but the overall structure of the mean flow is not significantly changed, see Figure 3. We focus on the velocity of the upwelling and downwelling jets to allow comparison with the literature where velocity is estimated with pairs of thermometers at mid-height [21–23]. In symmetrical cells, we average the velocity of the downwelling and upwelling jets. In RS cells, we associate the downwelling jet with the top plate, and the upwelling jet with the bottom plate. Indeed, we use the following definition for the Reynolds numbers, $Re_{r,s}$ of the rough bottom and the smooth top,

$$Re_{r,s} = \frac{U_{\text{up,down}} H}{\nu}, \tag{4}$$

where ν is the kinematic viscosity and $U_{\text{up,down}}$ is the maximum of the profile along x of vertical velocity in the plane at mid-height.

The Reynolds numbers in the various configurations, as well as those of the literature, show deviations, more than a factor 2, even when differences in the definition have been accounted for, see Figure 4-a. These deviations, though relatively small, are significant for quantities that scale with a power of the Reynolds number. For example, the Reynolds number in the RS cell using

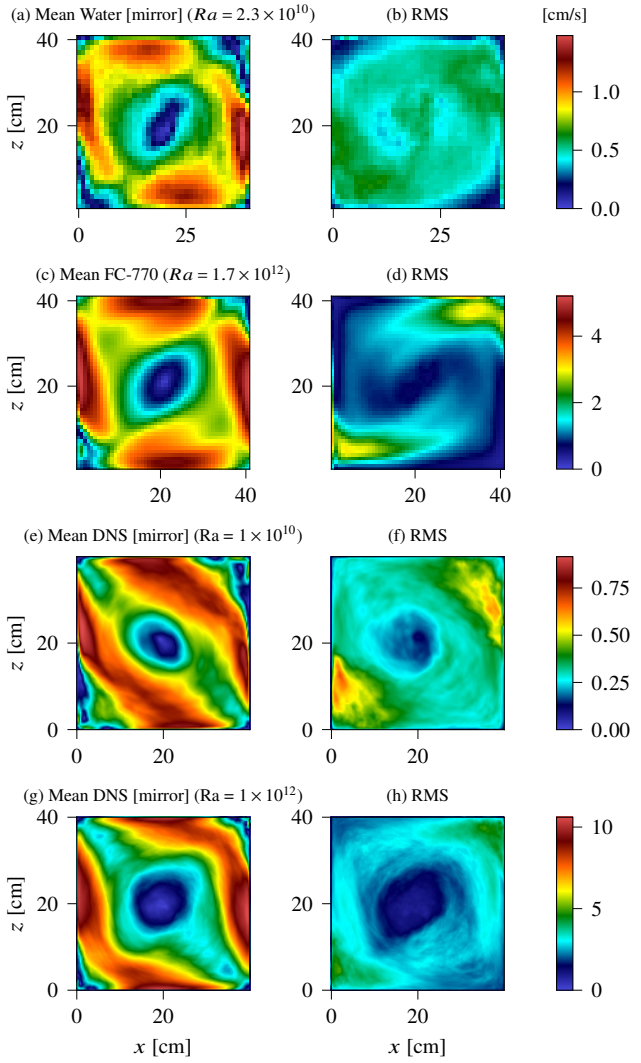

FIG. 2. Mean (a, c) and RMS (b, d) velocity maps computed from the Shadowgraph recording in smooth cells (SS), and from DNS velocity fields at mid-depth (e, f, g, h). (a, b) Water $Ra = 2.3\times10^{10}$, $Re = 5.4\times10^{3}$; (c, d) FC-770 $Ra = 1.7\times10^{12}$, $Re = 3.3\times10^{4}$; (e, f) DNS $\Gamma_{yz} = 0.25$, $Ra = 10^{10}$, $Re = 4.9\times10^{3}$; (g, h) DNS $\Gamma_{yz} = 0.25$, $Ra = 10^{12}$, $Re = 6.3\times10^{4}$.

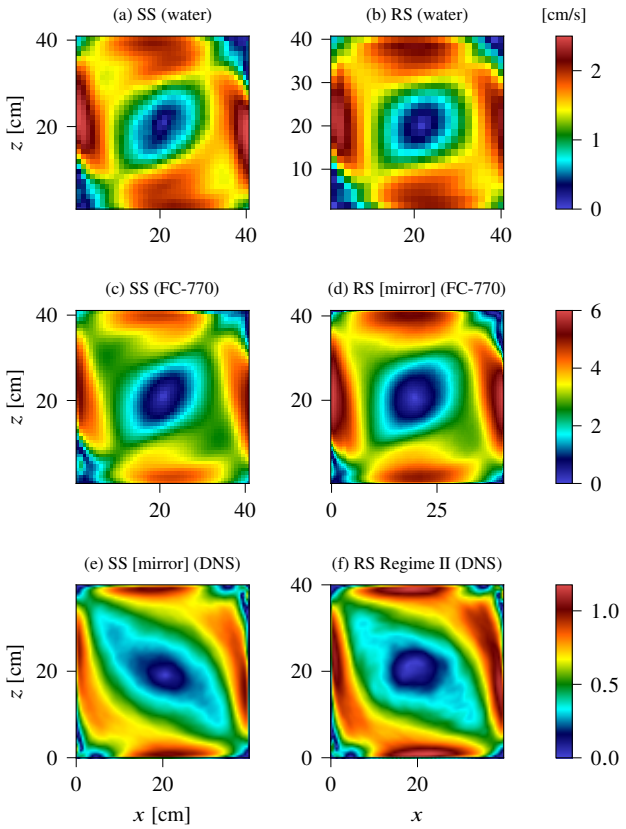

FIG. 3. Mean velocity maps computed from the experimental Shadowgraph in SS (a, c) and RS (b, d) configurations, as well as velocity maps from the DNS (e, f). (a) SS Water $Ra = 6.3\times10^{10}$, $Re = 1.6\times10^{4}$. (b) RS Water $Ra = 5.6\times10^{10}$, $Re = 1.4\times10^{4}$. (c) SS FC-770 $Ra = 1.7\times10^{12}$, $Re = 3.3\times10^{4}$. (d) RS FC-770 $Ra = 1.6\times10^{12}$, $Re = 4.0\times10^{4}$. (e) DNS $\Gamma_{yz} = 0.5$, $Ra = 10^{10}$, $Re = 5.7\times10^{3}$. (f) DNS $\Gamma_{yz} = 0.5$, $h_0 = 0.004$, $Ra = 10^{10}$, $Re = 6.3\times10^{3}$.

fluorocarbon is larger than in the SS case, and additionally is asymmetrical (velocity is larger near the rough plate). This Reynolds number enhancement triggered by roughness was not visible in our previous measurements using PIV in water at lower Prandtl and Rayleigh numbers [24]. Indeed, the Rayleigh number of the new data obtained in fluorocarbon is a decade larger and further from the threshold where roughness-enhanced heat-transfer is triggered than the rough cell using water. The higher Prandtl number also further separates the thermal and viscous boundary layers, which probably plays a role in the boundary layer response to plate roughness.

One interesting quantity is the friction coefficient,

$$\frac{RaNu}{Re^3Pr^2}, \tag{5}$$

which was used by Chavanne, *et al.* as an indicator of the transition to turbulence in the boundary layers [21], and can alternatively be interpreted as proportional to the ratio between the kinetic energy dissipation rate ϵ and the bulk energy dissipation rate $\epsilon_{u,bulk}$ [27],

$$\epsilon = \frac{\nu^3}{H^4}(Nu-1)RaPr^{-2}, \tag{6}$$

$$\epsilon_{u,bulk} \propto \frac{\nu^3}{H^4}Re^3. \tag{7}$$

In the range of parameters explored in this work, we evidence a transition at a critical Reynolds number, $Re_c \approx 10^4$. Beyond this transition, the friction coefficient no longer depends on the Reynolds number, or

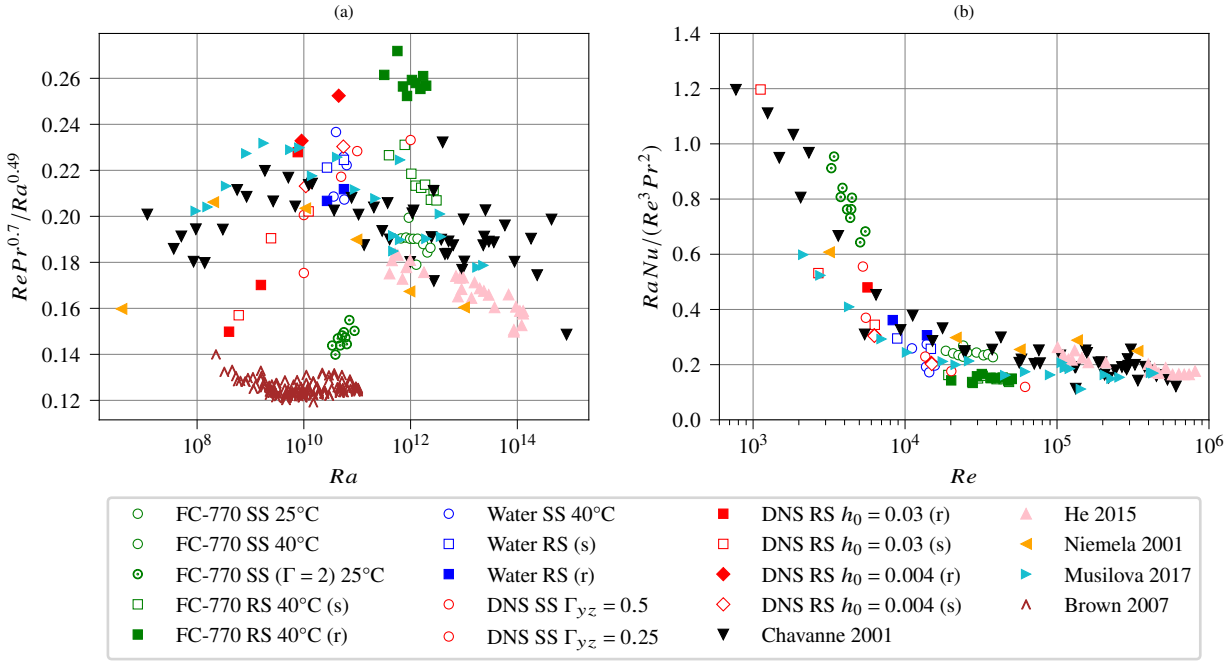

FIG. 4. (a) Reynolds number measurements in FC-770 (green), water (blue) and from DNS (red), in RS (squares) and SS (circles) cells. Data from [21–23, 25, 26] are plotted for comparison (triangles). (b) Friction coefficient for all data points (same symbols). The heat flux, $RaNu$ collapses for all data with $RaNu \sim 0.2Re^3Pr^2$.

only very weakly, see Figure 4-b. Therefore, we get a relationship between the dimensionless heat-flux, $RaNu$, and the Reynolds and Prandtl numbers, where

$$RaNu = \frac{g\rho^2\alpha C_p H^4}{\mu\lambda^2}\dot{q}. \tag{8}$$

The phenomenological relationship is,

$$RaNu \approx 0.2Re^3Pr^2. \tag{9}$$

However, this result does not allow to directly infer whether the kinetic energy dissipation rate is dominated by the bulk energy dissipation rate, or how much dissipation in the boundary layers still contributes, because of prefactors stemming from the non-unique definition for the Reynolds number and of the turbulent dissipation.

It is remarkable that this relationship, Eq. 9, holds for the Grenoble data which evidence a transition to the ultimate regime, as well as data which does not evidence such transition, and also in the case of rough cells in which $Nu \sim Ra^{1/2}$, as well as smooth cells with a classical scaling. This shows that whatever changes are triggered by either the roughness or the transition to the ultimate regime are entirely taken into account in the Reynolds number. While it may seem at first glance that the Reynolds number is only a function of Ra and Pr, it really is not. Multiple flows are possible at a given Rayleigh number [10, 28], and it is therefore elusive to try to determine a universal Nu *versus* Ra relationship. The universal scaling for the heat-flux, Eq. 9, evidenced in this work, has to be taken into account in tentative theoretical models of turbulent thermal convection.

ACKNOWLEDGMENTS

The authors are thankful to Marc Moulin and his team at the mechanical workshop for the design and machining of the experimental apparatus. This work was funded by ANR-18-CE30-0007-01 JCJC "CryoGrad", and by ANR-22-CE30-0018-01 PRC "Thermal" projects, and benefited from the resources of the PSMN computing center in Lyon. This project was provided with computing HPC and storage resources by GENCI at CINES and TGCC thanks to the grants 2022, 2023 and 2024-2A00326 on the supercomputer Joliot Curie's ROME and Adastra's GENOA partitions.

* julien.salort@ens-lyon.fr

[1] F. Chillà and J. Schumacher, New perspectives in turbulent Rayleigh-Bénard convection, Eur. Phys. J. E **35**, 58 (2012).

[2] R. J. A. M. Stevens, E. P. van der Poel, S. Grossmann, and D. Lohse, The unifying theory of scaling in thermal convection: the updated prefactors, J. Fluid Mech. **730**, 295 (2013).

[3] L.-A. Couston and M. Siegert, Dynamic flows create potentially habitable conditions in Antartic subglacial

lakes, Sci. Adv. **7**, eabc3972 (2021).
[4] R. H. Kraichnan, Turbulent thermal convection at arbitrary Prandtl number, Phys. Fluids **5**, 1374 (1962).
[5] X. Chavanne, F. Chillà, B. Castaing, B. Hébral, B. Chabaud, and J. Chaussy, Observation of the ultimate regime in Rayleigh-Bénard convection, Phys. Rev. Lett. **79**, 3648 (1997).
[6] J. J. Niemela and K. R. Sreenivasan, Confined turbulent convection, J. Fluid Mech. **481**, 355 (2003).
[7] X. He, D. Funfschilling, E. Bodenschatz, and G. Ahlers, Heat transport by turbulent Rayleigh-Bénard convection for $Pr \simeq 0.8$ and $4 \times 10^{11} < Ra < 2 \times 10^{14}$: ultimate-state transition for aspect ratio $\gamma = 1.00$, New J. Phys. **14**, 063030 (2012).
[8] J. J. Niemela, L. Skrbek, K. R. Sreenivasan, and R. J. Donnelly, Turbulent convection at very high Rayleigh numbers, Nature **404**, 837 (2000).
[9] P. Urban, P. Hanzelka, T. Králik, M. Macek, and V. Musilová, Elusive transition to the ultimate regime of turbulent rayleigh-bénard convection, Phys. Rev. E **99**, 011101(R) (2019).
[10] P.-E. Roche, F. Gauthier, R. Kaiser, and J. Salort, On the triggering of the ultimate regime of convection, New J. Phys. **12**, 085014 (2010).
[11] P.-E. Roche, The ultimate state of convection: a unifying picture of very high Rayleigh numbers experiments, New J. Phys. **22**, 073056 (2020).
[12] G. Ahlers, E. Bodenschatz, R. Hartmann, X. He, D. Lohse, P. Reiter, R. J. A. M. Stevens, R. Verzicco, M. Wedi, S. Weiss, X. Zhang, L. Zwirner, and O. Shishkina, Aspect ratio dependence of Heat transfer in a Cylindrical Rayleigh-Bénard cell, Phys. Rev. Lett. **128**, 084501 (2022).
[13] D. Lohse and O. Shishkina, Ultimate turbulent thermal convection, Phys. Today **76**, 26 (2023).
[14] L. Méthivier, R. Braun, F. Chillà, and J. Salort, Turbulent transition in Rayleigh-Bénard convection with fluorocarbon, EPL **136**, 10003 (2021).
[15] M. Belkadi, A. Sergent, Y. Fraigneau, and B. Podvin, On the role of roughness valleys in turbulent rayleigh-bénard convection, J. Fluid Mech. **923**, 10.1017/jfm.2021.583 (2021).
[16] M. Belkadi, L. Guislain, A. Sergent, B. Podvin, F. Chillà, and J. Salort, Experimental and numerical shadowgraph in turbulent Rayleigh-Bénard convection with a rough boundary: investigation of plumes, J. Fluid Mech. **895**, A7 (2020).
[17] J.-C. Tisserand, M. Creyssels, Y. Gasteuil, H. Pabiou, M. Gibert, B. Castaing, and F. Chillà, Comparison between rough and smooth plates within the same Rayleigh-Bénard cell, Phys. Fluids **23**, 015105 (2011).
[18] E. Rusaouen, O. Liot, J. Salort, B. Castaing, and F. Chillà, Thermal transfer in Rayleigh-Bénard cell with smooth or rough boundaries, J. Fluid Mech. **837**, 443 (2018).
[19] J. Salort, O. Liot, E. Rusaouen, F. Seychelles, J.-C. Tisserand, M. Creyssels, B. Castaing, and F. Chillà, Thermal boundary layer near roughnesses in turbulent Rayleigh-Bénard convection: flow structure and multistability, Phys. Fluids **26**, 015112 (2014).
[20] Y.-C. Xie and K.-Q. Xia, Turbulent thermal convection over rough plates with varying roughness geometries, J. Fluid Mech. **825**, 573 (2017).
[21] X. Chavanne, F. Chillà, B. Chabaud, B. Castaing, and B. Hébral, Turbulent Rayleigh-Bénard convection in gaseous and liquid he, Phys. fluids **13**, 1300 (2001).
[22] X. He, D. P. M. van Gils, E. Bodenschatz, and G. Ahlers, Reynolds numbers and the elliptic approximation near the ultimate state of turbulent Rayleigh-Bénard convection, New J. Phys. **17**, 063028 (2015).
[23] J. J. Niemela, L. Skrbek, K. R. Sreenivasan, and R. J. Donnelly, The wind in confined thermal convection, Journal of Fluid Mechanics **449**, 169 (2001).
[24] O. Liot, Q. Ehlinger, E. Rusaouën, T. Coudarchet, J. Salort, and F. Chillà, Velocity fluctuations and boundary layer structure in a rough Rayleigh-Bénard cell filled with water, Phys. Rev. Fluids **2**, 044605 (2017).
[25] V. Musilová, T. Králik, M. L. Mantia, M. Macek, P. Urban, and L. Skrbek, Reynolds number scaling in cryogenic turbulent rayleigh-bénard convection in a cylindrical aspect ratio one cell, J. Fluid Mech. **832**, 721 (2017).
[26] E. Brown, D. Funfschilling, and G. Ahlers, Anomalous reynolds-number scaling in turbulent rayleigh-bénard convection, J. Stat. Mech. , P10005 (2007).
[27] S. Grossmann and D. Lohse, Scaling in thermal convection: a unifying theory, J. Fluid Mech. **407**, 27 (2000).
[28] P.-E. Roche, *Convection thermique turbulente en cellule de Rayleigh-Bénard cryogénique*, Ph.D. thesis, Université Joseph-Fourier (2001).